Synergy of random balance design method and intelligent optimization technique for model updating of the 4MW offshore wind turbine benchmark

Kai Xu[a], Ankang Meng[a], Shuang Chang[a,b], Dianzi Liu[a,c], Fushun Liu[a,b,*]

[a] *College of Engineering, Ocean University of China, Qingdao 266100 , China*
[b] *Shandong Province Key Laboratory of Ocean Engineering, Ocean University of China, Qingdao 266100, China*
[c] *School of Engineering, University of East Anglia, Norwich, NR14 7TH, United Kingdom*

Abstract

The technical challenges for model updating of real marine engineering structures include the extraction of modal parameters associated with incomplete measurement information and the correction of a large number of structural parameters. As it is difficult to verify the effectiveness of model updating methods for engineering applications, the representative models have to be adopted in finite element (FE) analysis or lab-scale tests, leading to the incomplete reflection of actual structural performances. Based on these factors, a practical model updating method is developed in this study to make full use of field measurement data from a 4MW offshore wind turbine for the accurate estimation of structural parameters using the random balance designs-Fourier amplitude sensitivity test (RBD-FAST) strategy and an improved particle swarm optimization (IPSO). Leveraging the measured acceleration signals from offshore wind turbines under the conditions including operation, shutdown, collision and typhoon scenarios, the complex exponential decomposition method is applied to accurately extract the time-varying acceleration components (TVAC) for the construction of the frequency response function (FRF). Following that, RBD-FAST is implemented into IPSO with adaptive inertia weights and asynchronously varying learning factors to enable efficient selection of numerous updated physical parameters, thus improving time cost and computational accuracy. The correctness of the proposed method is verified by a numerical jacket platform model. Furthermore, the 4MW offshore wind turbine benchmark is developed to assess the feasibility of the proposed model updating method using field measured data from different scenarios. Results show that the synergy of RBD-FAST and IPSO in the proposed method can accurately update parameters and minimize a maximum discrepancy of 0.8970% for the first-three orders of natural frequencies between the benchmark and the updated models in the collision scenario. Summarily, the present work provides a potential technique and practical engineering references for model updating of offshore wind turbines subject to harsh marine environments.

Keywords:
Model updating; Field measured data; Offshore wind turbine; Random balance design; Improved particle swarm optimization

*Corresponding author.
Email address: percyliu@ouc.edu.cn (Fushun Liu)

Nomenclature		p_i	Input parameters
$\bar{a}_{lr}$	Amplitude of normalized TVAC	P, P_g	Local and global optima of the particles
A_j, B_j	Coefficients of Fourier series	$s_{\sigma r}$	Random permutation vector
c_1, c_2	Learning factors	$\boldsymbol{SAC}$	Signature assurance criterion
$\boldsymbol{C}_0$, $\mathbf{C}^*$	Global damping matrices of reference and benchmark models	S_i	First-order sensitivity index
D	Total variance	T	Transpose of matrices
f_c, f_{avg} , f_{min}	Current, mean and minimum values of all particles	$\mathbf{u}$	Displacement vector
$\mathbf{f}$	Excitation vector	$\mathbf{v}$	Velocity of the particles
$\boldsymbol{F}_c$	Cost function	$\mathbf{x}$	Position of the particles
G_i	Transformation function	y	Model output
$H_{a^*}^{pl}$	Acceleration FRF	$Y\left(s_j\right)$	Amplitude of Fourier transform
$\mathbf{I}$	Identity matrices	α_r, β_r, γ_r	Variation coefficients of mass, stiffness and damping
J	Imaginary unit	Λ_j	Mode of Fourier series
k	Number of input parameters	$\mathbb{C}_{\text{ranking}}$	Ranked variation coefficients
$\boldsymbol{K}_0$, $\mathbf{K}^*$	Global siffness matrices of reference and benchmark models	ϕ_i	Random phase-shift
M	Interference factor	ϕ_{lr}	Mode shapes
$\boldsymbol{M}_0$, $\mathbf{M}^*$	Global mass matrices of reference and benchmark models	ω_i	Harmonic frequency
N	Sample size	$\hat{\omega}$	Inertia weight
N_a	Number of degrees of freedom	$\widehat{\omega}_{\text{max}}$, $\widehat{\omega}_{\text{min}}$	Maximum and minimum values of the inertia weight
N_m	Number of sensors		

1. Introduction

Model updating of offshore structures is critically important to eliminate differences in physical parameters caused by designs, constructions, corrosion, ageing and adhesions of sea life. In general, model updating methods for offshore structures have relied on numerical [1] or small-scale experimental models [2], which only provide the virtual and simplified references. As compared to the above methods, the model updating approaches based on field measured data reflecting complex loads and structural prototypes have become the future trend, as the corrected results have the ability to demonstrate the real physical characteristics well. However, the applications of field-based model updating methods have rarely been investigated due to noise interference [3], unstable loads boundary conditions [4], incomplete measurement information [5], and dynamically changing structures [6, 7] under complex marine environments. Although such challenges exist, the pursuit of high-fidelity model updating based on limited field data has still received increasingly attention.

Model updating methods can be divided into matrix-type and parameter-type methods according to the target object. The matrix-based method was first investigated by Berman [8, 9] and Baruch [10, 11], and the FE model was updated with the stiffness and mass matrices of structures. In these approaches, the model was updated by weighting the Euclidean sense, and direct and iterative computing forms were defined and discussed. However, original banding and sparse characteristics of the mass and stiffness matrices were no longer maintained due to insufficient constraints. As compared to the matrix-based method, updating parameters including material density, modulus of elasticity and geometry of the structure, etc., in the parameter-type updating method have the clearer physical meaning owing to the direct reflection of structural properties. Furthermore, the corrected parameters can also be the submatrices, which described real subsystems and assembly of interface elements of subsystems [12]. Then the experimental model was obtained by multiplying submatrices units of the mass and stiffness matrices with the correction factors.

The parameter-type method normally transforms the model updating into an optimization problem accompanied by the selection of the objective function, the calculation of sensitivity and the iteration of the correction parameters. In the optimization process, the objective function constructed from the modal parameters is extremely important to ensure the accuracy of the results [13–15]. With the development of modal parameter identification technique, the natural frequency [16], mode shape [17] and mode shape curvature [18, 19] of structures have been effectively extracted based on the structural vibration signal. Naranjo-Perez et al. [20] improved the FE model updating for civil engineering structures by collaborative machine learning-optimization algorithms based on established multiple objective functions related to natural frequencies and vibration modes. Tiwary et al. [21] explored the effective dimensionality of the model updating problem using Causal Bayesian Optimization. The obtained mode shapes between experimental and predicted models were also compared using modal assurance criterion (MAC) percentages. However, during the service life of offshore structures, the environmental loads are complex and varied, and vibration monitoring data is insufficient and easily disturbed by noise, making the identification of modal parameters difficult. Moreover, studies indicated that only limited low-order modal information could be extracted from the measured vibration signals of structures, and the identification of high-order modal parameters was not accurate [22]. As compared to the modal parameters, the FRF obtained by experimental testing was less sensitive to measurement errors and more sensitive to variations of structural parameters [23]. Therefore, the FRF for model updating effectively

reduced errors that caused by modal parameter identification and model reduction [24]. Moreover, multiple FRF curves were constructed in use of a finite number of vibration monitoring locations and sufficient information was provided due to their wide frequency ranges [25, 26]. Based on these advantages of FRFs, the pathological problem of the matrix due to the number of equations constructed being smaller than that of the correction parameters was also solved. Wang et al. [27] proposed a model updating method based on the acceleration FRF to improve the computational efficiency by introducing the Kriging model as a metamodel in the optimization process. Prendergast et al. [28] determined the mobilised soil stiffness and mass profiles by the iterative updating of two experimental piles. In the developed approach, the FRF in objective functions were obtained from an impact test performed on a test pile. Fathi et al. [5] investigated a new Bayesian model updating framework using incomplete FRF data. Authors claimed that the incomplete measurements issue was addressed by using FRF at different excitation frequencies to increase the number of data in the objective function.

Although great progress on the parameter-type updating methods has been made, there are still some limitations to be addressed. For example, the sensitivity calculations are complicated and time-consuming to update numerous parameters in the engineering applications using parameter-based methods. To improve the stability and efficiency of the model updating process, the Sobol sensitivity analysis method was applied to determine the important modal parameters [29]. Zhong and Chen [30] performed the Sobol global sensitivity analysis for the hybrid model updating in order to obtain sensitivity indices of parameters that change with time. Similarly, sensitivity analysis techniques such as Fourier amplitude sensitivity test (FAST) and Random balance designs (RBD)-FAST [31, 32] were used to identify main influencing factors in the model. Furthermore, the assumptions and performance of the function-weighted FRF sensitivities were investigated [33]. Zhu et al. [34] proposed a frequency-domain nonlinear model updating method based on analytical sensitivity, which can significantly reduce the time for iterations in model updating process. These advanced studies have shown that the parameter selection of model updating using the sensitivity analysis is crucial to reduce the time costs of model updating.

In this paper, a novel hybrid approach to the synergy of RBD-FAST and intelligent IPSO has been proposed for model updating with numerous parameters using the on-site measured data from the 4MW offshore wind turbine under multiple service conditions. The completeness of the extracted modal features has been improved by the combination of the TVAC and theoretical mode shapes. The paper has been organized as follows: Section 2 has provided a detailed mathematical description of the underlying theory of FAST, along with a discussion of its limitations. In Section 3, the theoretical derivation of the RBD-FAST based IPSO by incorporating the TVAC with theoretical mode shapes has been carried out. In Section 4, the correctness of the proposed approach has been demonstrated by numerical examples of the jacket platform model. In Section 5, the feasibility of the proposed model updating approach has been investigated using the measured acceleration data from a 4MW offshore wind turbine benchmark. Finally, potential research on model updating of marine engineering structures using the proposed method has been summarized in Section 6.

2. Preliminary of sensitivity analysis

As evaluating the effects of all input parameters on the high-dimensional parametric system is complicated and time-consuming, it is necessary to identify the key input variables through sensitivity analysis. The Fourier amplitude

sensitivity test (FAST) has demonstrated the ability to determine the first-order sensitivity of different input parameters for quantifying the respective importance of input factors. Suppose the number k of input parameters in the model space are $p_1, p_2, p_3, \cdots, p_k$ and the output y can be defined in a form of Eq. (1) as follows:

$$y = f(p) = f\left(p_1, p_2, \cdots, p_k\right) \tag{1}$$

Firstly, the transformation function G_i is introduced to parameterize p_i:

$$\begin{cases} p_i\left(s_j\right) = G_i\left(\sin\left(\omega_i s_j + \phi_i\right)\right), \quad i = 1, 2, \ldots, k \\ s_j = -\pi + \frac{2j\pi}{N}, \quad j = 1, 2, \ldots, N \end{cases} \tag{2}$$

where ω_i represents the harmonic frequency for the ith input parameter, ϕ_i means a random phase-shift and N denotes the sample size.

First-order sensitivity index S_i for the parameter p_i based on the variance calculation can be defined as:

$$\begin{cases} S_i = \frac{V_i}{V} = \frac{\sum_{n=1}^{M} \Lambda_{n\omega_i}}{\sum_{n=1}^{N/2} \Lambda_n} \\ \Lambda_n = \frac{1}{N^2} Y\left(s_j\right)^2 \left(\left\{ \sum_{j=1}^{N} \cos\left(n s_j\right) \right\}^2 + \left\{ \sum_{j=1}^{N} \sin\left(n s_j\right) \right\}^2 \right) \end{cases} \tag{3}$$

where V_i is the variance corresponding to the parameter p_i and V denotes the total variance. M represents the predefined integer called the interference factor, $\Lambda_{n\omega_i}$ means the mode of Fourier series for the ith input parameter at the harmonics of ω_i, and $Y\left(s_j\right)$ is the corresponding amplitude of Fourier transform of the output signal $y\left(s_j\right)$.

As the maximum harmonic frequency is proportional to the number of input factors k shown in Eq. (2), the computational cost of sensitivity analysis remains prohibitive for the complex structures, which limits the engineering application of the FAST method.

3. The developed sensitivity-based optimization method

The dynamic behavior of the FE model for marine engineering structures with the N_a degrees of freedom is governed by a set of differential equations. The excitation vector $\mathbf{f}(t)$ and the corresponding displacement vector $\mathbf{u}(t)$ in Eq. (4) are defined as the input and output of the dynamic system, respectively.

$$\mathbf{M}^*\left(\alpha_r\right)\ddot{\mathbf{u}}(t) + \mathbf{K}^*\left(\beta_r\right)\mathbf{u}(t) + \mathbf{C}^*\left(\gamma_r\right)\dot{\mathbf{u}}(t) = \mathbf{f}(t) \tag{4}$$

where $\mathbf{M}^*\left(\alpha_r\right)$, $\mathbf{K}^*\left(\beta_r\right)$ and $\mathbf{C}^*\left(\gamma_r\right) \in \mathbb{R}^{N_a \times N_a}$ represent the global mass, stiffness and damping matrices of the benchmark model[1], respectively.

Subsequently, the global matrices can be defined in the form of submatrices and variation coefficients α_r, β_r and γ_r as follows:

$$\begin{cases} \mathbf{M}^*\left(\alpha_r\right) = \mathbf{M}_0 + \sum_{r=1}^{N_a} \alpha_r \mathbf{M}_r \\ \mathbf{K}^*\left(\beta_r\right) = \mathbf{K}_0 + \sum_{r=1}^{N_a} \beta_r \mathbf{K}_r \\ \boldsymbol{C}^*\left(\gamma_r\right) = \boldsymbol{C}_0 + \sum_{r=1}^{N_a} \gamma_r \boldsymbol{C}_r \end{cases} \tag{5}$$

[1] Actual marine engineering structures or actual objects for model updating

where $\mathbf{M}_0$, $\mathbf{K}_0$ and $\boldsymbol{C}_0$ represent the global mass, stiffness and damping matrices of the reference model, respectively. $\mathbf{M}_r$,$\mathbf{K}_r$ and $\boldsymbol{C}_r$ denote the rth mass, stiffness and damping submatrices of the element for the reference model, respectively.

3.1. Optimized cost function based on TVAC

Model updating could essentially be translated into an optimization problem of the correction parameters by minimizing the discrepancy between the measured and calculated data in the cost function. In practical engineering applications, it is difficult to accurately obtain modal parameters of marine structures for the cost function due to the severe marine environments and the limitation on the number of sensors. As the complex exponential method has the ability to effectively eliminate the influence of factors, such as loads and noise, on structural vibration responses, the TVAC corresponding to structural characteristics can be accurately extracted from the measured accelerations [35]. Furthermore, the TVAC is normalized to construct the acceleration FRF $H_{a^*}^{pl}(\omega)$ in Eq. (6), which representing the relationship between the load point l and the response point p.

$$H_{a^*}^{pl}(\omega) = \sum_{r=1}^{N_a} \frac{-\omega^2 \bar{a}_{lr} \bar{a}_{pr}}{-M_{r^*}\omega^2 + JC_{r^*}\omega + K_{r^*}} \tag{6}$$

where $\bar{a}_{lr}$ and $\bar{a}_{pr}$ are amplitudes of the lth and pth elements in the rth normalized TVAC, respectively. J means the imaginary unit.

It is noted that incomplete measurements are unavoidable due to the difficulty in extracting higher order mode shapes to construct the FRFs of marine structures. Therefore, a complete library of modal shapes has been established to address the challenge of incompleteness of the measured FRFs in this study. More specifically, the lower order modal features are extracted by normalizing the TVAC of the benchmark model, while the higher order modal shapes are obtained from the theoretical analysis of the reference model. The acceleration FRFs of the benchmark model can be rewritten as:

$$\hat{H}_{a^*}^{pl}(\omega) \cong \sum_{r=1}^{N_m} \frac{-\omega^2 \bar{a}_{lr} \bar{a}_{pr}}{-M_{r^*}\omega^2 + j_a C_{r^*}\omega + K_{r^*}} + \sum_{r=N_m+1}^{N_a} \frac{-\omega^2 \phi_{lr} \phi_{pr}}{-M_{r^*}\omega^2 + j_a C_{r^*}\omega + K_{r^*}} \tag{7}$$

where N_m is the number of degrees of freedom for sensors mounted on the structure. ϕ_{lr} and ϕ_{pr} are the rth mode shapes at the element l and element p, respectively.

Substituting Eq. (5) into Eq. (7) and ignoring the update of the damping property, one has:

$$\begin{aligned} \hat{H}_{a^*}^{pl}(\alpha_r, \beta_r, \omega) \cong & \sum_{r=1}^{N_m} \frac{-\omega^2 \bar{a}_{lr} \bar{a}_{pr}}{(M_0 + \alpha_r M_r)\omega^2 + (K_0 + \beta_r K_r) + j_a (C_0)\omega} \\ & + \sum_{r=N_m+1}^{N_a} \frac{-\omega^2 \phi_{lr} \phi_{pr}}{-(M_0 + \alpha_r M_r)\omega^2 + (K_0 + \beta_r K_r) + j_a (C_0)} \end{aligned} \tag{8}$$

To establish the correlation of the FRFs between the benchmark and reference models, the signature assurance criterion (SAC) of $H_a^{pl}(\omega)$ for the offshore structures is defined by Eq. (9):

$$SAC_{pl}(\alpha_r, \beta_r) = \frac{\left(\left| \left\{ \hat{H}_{a^*}^{pl}(\alpha_r, \beta_r, \omega) \right\}^T \left\{ H_a^{pl}(\omega) \right\} \right| \right)^2}{\left(\left\{ \hat{H}_{a^*}^{pl}(\alpha_r, \beta_r, \omega) \right\}^T \left\{ \hat{H}_{a^*}^{pl}(\alpha_r, \beta_r, \omega) \right\} \right) \left(\left\{ H_a^{pl}(\omega) \right\}^T \left\{ H_a^{pl}(\omega) \right\} \right)} \tag{9}$$

where the symbol T represents the transpose of the matrix.

Similarly, the SAC matrix of FRFs $H_a(\omega)$ for the marine structure can be expressed as follows:

$$\boldsymbol{SAC}\left(\boldsymbol{\alpha}_r, \boldsymbol{\beta}_r\right) = \begin{bmatrix} SAC_{11}\left(\alpha_r, \beta_r\right) & SAC_{12}\left(\alpha_r, \beta_r\right) & \cdots & SAC_{1N_a}\left(\alpha_r, \beta_r\right) \\ SAC_{21}\left(\alpha_r, \beta_r\right) & SAC_{22}\left(\alpha_r, \beta_r\right) & \cdots & SAC_{2N_a}\left(\alpha_r, \beta_r\right) \\ \cdots & \cdots & \cdots & \cdots \\ SAC_{N_a1}\left(\alpha_r, \beta_r\right) & SAC_{N_a2}\left(\alpha_r, \beta_r\right) & \cdots & SAC_{N_aN_a}\left(\alpha_r, \beta_r\right) \end{bmatrix} \tag{10}$$

Based on the SAC matrix and the natural frequencies, the cost function for evaluating the discrepancy between the benchmark and reference models can be formulated by Eq. (11).

$$\boldsymbol{F}_c = \left\{ \sum_{r=1}^{N_m} \left(\mathbf{I} - \boldsymbol{SAC}\left(\boldsymbol{\alpha}_r, \boldsymbol{\beta}_r\right) \right) \right\} + \left\{ \sum_{r=1}^{N_m} \frac{\left| \omega_r\left(\alpha_r, \beta_r\right) - \omega_{r^*} \right|}{\omega_r\left(\alpha_r, \beta_r\right)} \right\} \tag{11}$$

where ω_{r^*} and $\omega_r\left(\alpha_r, \beta_r\right)$ are natural frequencies of the benchmark and reference models, respectively. $\mathbf{I} \in \mathbb{R}^{N_a \times N_a}$ is the identity matrix.

3.2. Improved particle swarm optimization (IPSO)

Particle swarm optimization has the power to find the global optimal solution by simply adjusting the trajectory of each individual to its own optimal position and the optimal particle of the entire swarm [36]. For a N_a dimensional search space, the position $\mathbf{x}$ and velocity $\mathbf{v}$ of the particle at t to $t+1$ iterations can be determined by Eq. (12), assuming no change in the damping coefficients.

$$\begin{array}{cccc} \mathbf{x}(t) & \mathbf{v}(t) & \mathbf{x}(t+1) & \mathbf{v}(t+1) \\ \begin{bmatrix} \alpha_1^x(t) \\ \alpha_2^x(t) \\ \vdots \\ \alpha_{N_a}^x(t) \end{bmatrix} \begin{bmatrix} \alpha_1^v(t) \\ \alpha_2^v(t) \\ \vdots \\ \alpha_{N_a}^v(t) \end{bmatrix} & \Rightarrow & \begin{bmatrix} \alpha_1^x(t+1) \\ \alpha_2^x(t+1) \\ \vdots \\ \alpha_{N_a}^x(t+1) \end{bmatrix} \begin{bmatrix} \alpha_1^v(t+1) \\ \alpha_2^v(t+1) \\ \vdots \\ \alpha_{N_a}^v(t+1) \end{bmatrix} \\ \begin{bmatrix} \beta_1^x(t) \\ \beta_2^x(t) \\ \vdots \\ \beta_{N_a}^x(t) \end{bmatrix} \begin{bmatrix} \beta_1^v(t) \\ \beta_2^v(t) \\ \vdots \\ \beta_{N_a}^v(t) \end{bmatrix} & \Rightarrow & \begin{bmatrix} \beta_1^x(t+1) \\ \beta_2^x(t+1) \\ \vdots \\ \beta_{N_a}^x(t+1) \end{bmatrix} \begin{bmatrix} \beta_1^v(t+1) \\ \beta_2^v(t+1) \\ \vdots \\ \beta_{N_a}^v(t+1) \end{bmatrix} \end{array} \tag{12}$$

In the $t+1$th iteration, the update of the particle position and velocity can be defined as:

$$\begin{cases} \mathbf{x}(t+1) = \mathbf{x}(t) + \mathbf{v}(t+1) \\ \mathbf{v}(t+1) = \hat{\omega}\mathbf{v}(t) + c_1(P - \mathbf{x}(t)) + c_2\left(P_g - \mathbf{x}(t)\right) \end{cases} \tag{13}$$

where $\hat{\omega}$ represents the inertia weight. c_1 and c_2 are the learning factors. P and P_g denote the local and global optima of the particles in the tth iteration, respectively.

The local and global optimality of the particles are influenced by the inertia weight $\hat{\omega}$. The perturbation of the particle trajectory by the empirical information between the particle itself and other particles depends on the learning

factors c_1 and c_2, respectively. The balance between global and local search can be achieved by dynamically changing inertia weights, which are defined as:

$$\widehat{\omega} = \begin{cases} \widehat{\omega}_{\text{min}} - \frac{(\widehat{\omega}_{\text{max}} - \widehat{\omega}_{\text{min}}) * (f_c - f_{\text{min}})}{f_{\text{avg}} - f_{\text{min}}}, & f_c \leqslant f_{\text{avg}} \\ \widehat{\omega}_{\text{max}}, & f_c > f_{\text{avg}} \end{cases} \tag{14}$$

where $\widehat{\omega}_{\text{max}}$ and $\widehat{\omega}_{\text{min}}$ represent the maximum and minimum values of the inertia weight, respectively. f_c, f_{avg} and f_{min} represent the current, mean and minimum values of all particles, respectively.

To achieve dynamic learning capability, asynchronously varying learning factors have been introduced into the PSO. Initially, the particles have been endowed with the values representing the great self-learning ability and weak social learning ability, leading to the enhanced global search capacity. Then, the greater social learning ability and weaker self-learning capacity that have facilitated the convergence to the global optimum, have been assigned to the particles. The formulas for the asynchronously variation of learning factors have been defined as follows:

$$\begin{cases} c_1 = c_{1,ini} + \frac{c_{1,fin} - c_{1,ini}}{t_{max}} * t \\ c_2 = c_{2,imi} + \frac{c_{2,fin} - c_{2,imi}}{t_{max}} * t \end{cases} \tag{15}$$

where $c_{1,ini}$ and $c_{2,ini}$ represent the initial values of c_1 and c_2, respectively. $c_{1,fin}$ and $c_{1,fin}$ are the final values of learning factors and t_{max} denotes the maximum number of iteration.

3.3. Parameter sensitivity analysis based on RBD-FAST

In IPSO method introduced in Section 3.2, the selection of updated parameters is critically important and influences the accuracy of optimal results. Therefore, the strategy for parameter sensitivity analysis using RBD-FAST has been developed. Based on Eq. (11), the cost function, the cost function $\boldsymbol{F}_c$ can be defined as a function of variation coefficients:

$$\boldsymbol{F}_c = f\left(\alpha_1, \alpha_2, \cdots, \alpha_{N_a}, \beta_1, \beta_2, \cdots, \beta_{N_a}\right) \tag{16}$$

According to Eq. (2), the parameterized α_r and β_r are formulated by Eq. (17):

$$\left[\alpha_r\left(s_j\right), \beta_r\left(s_j\right)\right] = G_r\left(\sin\left(\omega_r s_j + \phi_r\right)\right), \quad r = 1, 2, \ldots, N_a \tag{17}$$

To reduce the computational cost in solving Eq. (2), ω_r has been assigned the predefined value of ω and the input variables have been distinguished by a random permutation of the sampling point coordinates by RBD. Thus, α_r and β_r can be rewritten as:

$$\left[\alpha_r\left(s_{\sigma r}\right), \beta_r\left(s_{\sigma r}\right)\right] = G_r\left(\sin\left(\omega s_{\sigma r}\right)\right), \quad r = 1, 2, \ldots, N_a \tag{18}$$

where $s_{\sigma r}$ is the rth random permutation vector distributed over the vector spaces from $-\pi$ to π with N equally distant sampling points.

Furthermore, the model output $\boldsymbol{F}_c(s_{\sigma r})$ corresponding to the randomly permutated vector $s_{\sigma r}$ has been calculate and reordered such that the sampling points are in increasing order with respect to the initial variation coefficients. Then, the reorder output $\boldsymbol{F}_c(s_{\sigma r})$ can be expanded by Fourier series as follows:

$$\begin{cases} \boldsymbol{F}_c(s_{\sigma r}) = \sum_{j=-N}^{j=N} \{A_j \cos j s_{\sigma r} + B_j \sin j s_{\sigma r}\} \\ A_j = \frac{1}{N} \sum_{j=1}^{N} \cos\left(j s_{\sigma r}\right) \boldsymbol{F}_c(s_{\sigma r}) \\ B_j = \frac{1}{N} \sum_{j=1}^{N} \sin\left(j s_{\sigma r}\right) \boldsymbol{F}_c(s_{\sigma r}) \end{cases} \tag{19}$$

where A_j and B_j denote coefficients determined by Fourier series.

Subsequently, the magnitude of Fourier series Λ_j at the jth sampling point can be expressed as:

$$\Lambda_j = 1/2\left(A_j^2 + B_j^2\right) \tag{20}$$

The variance D_r of the rth parameter and the total variance D can be formulated as:

$$\begin{cases} D_r = \sum_{n=1}^{M} \Lambda_{nw} \\ D = \sum_{n=1}^{N/2} \Lambda_n \end{cases} \tag{21}$$

Finally, the first-order sensitivity index $\hat{S}_r$ of variation coefficients can be calculated by Eq. (22).

$$\hat{S}_r = D_r / D \tag{22}$$

The detailed procedure to perform RFD-FAST for the calculation of the first-order sensitivity index of each variation coefficients has been described as follows:

Step 1: Random permutation vector $s_{\sigma r}$ is selected in the vector space with N equally distant sampling points.

Step 2: To calculate the variation coefficients $\alpha_r\left(s_{\sigma r}\right)$ and $\beta_r\left(s_{\sigma r}\right)$ using the same frequency ω.

Step 3: To shuffle the variation coefficients $\alpha_r\left(s_{\sigma r}\right)$ and $\beta_r\left(s_{\sigma r}\right)$, calculate and reorder the output $\boldsymbol{F}_c(s_{\sigma r})$.

Step 4: To compute the first-order sensitivity index $\hat{S}_r$ using Eqs. (20 $\sim$ 22).

Summarily, a flowchart of model updating illustrating the proposed approach to the synergy of RFD-FAST and IPSO is provided in Fig. 1.

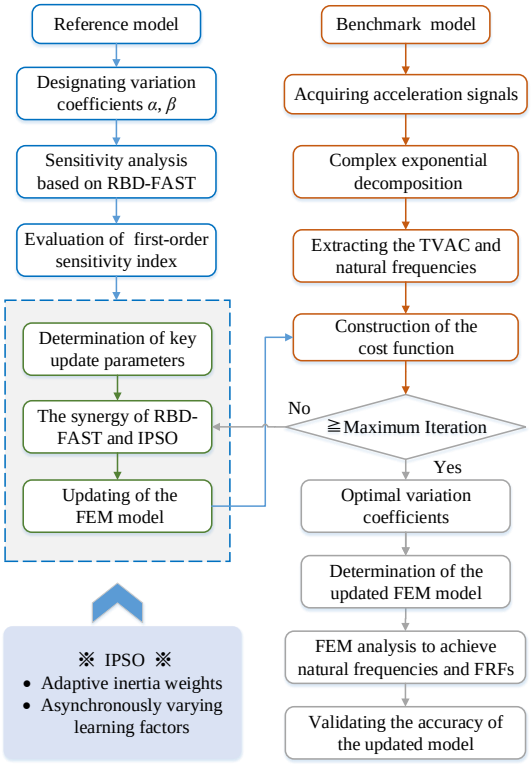

Fig. 1: Flowchart of model updating.

4. Numerical study of a jacket platform

To demonstrate the correctness and effectiveness of the synergy of RBD-FAST and intelligent IPSO in the proposed method, the numerical example of a jacket platform has been developed for this study. The numerical model established in MATLAB 2016a is composed of 48 elements, and the node of each element includes 3 translational and 3 rotational degrees of freedom. The dimensions including the model height, the length and width of top and bottom rectangular frames are 21.5m, 10.22m, 7.22m, 14.52m and 11.52m, respectively. The leg members of the jacket platform at 6m below the sea level are fully fixed. The Young's modulus, Poisson's ratio and density of the structure are 2.1×10^{11} Pa, 0.3 and 7850 kg/m^3, respectively. To generate the damage model of the jacket platform, five bars labeled as 29, 31, 42, 44 and 48 have been preset to represent the stiffness damage as shown in Fig. 2(b). Meanwhile, three bars labeled as 17, 20 and 21 have been expected for the mass update. During the model updating, the intact jacket platform as the reference model has been used to measure the degree of damage for the preset 'unhealthy' model.

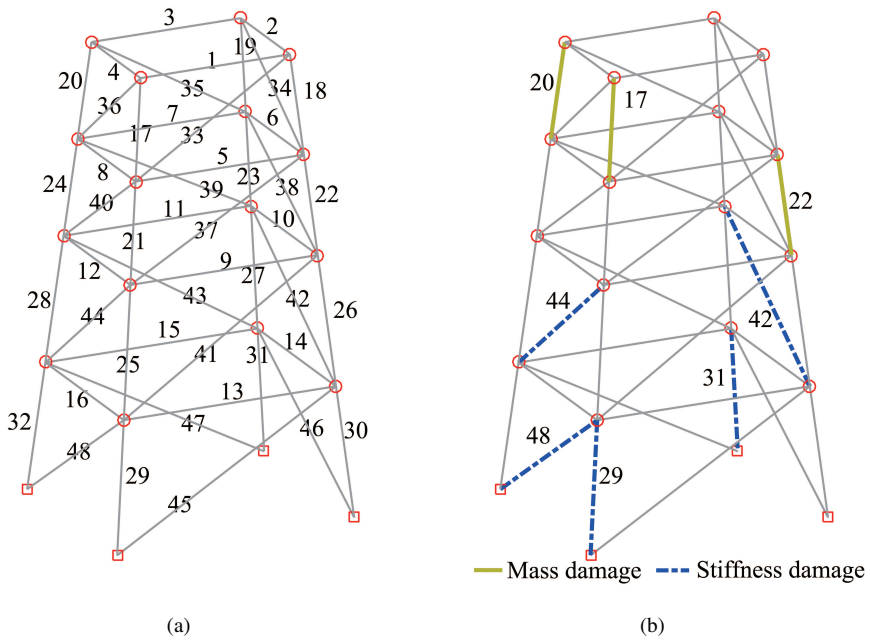

(a) (b)

Fig. 2: The jacket platform model: (a) The intact jacket platform model, (b) The damaged jacket platform model.

4.1. Frequency selection strategy of FRFs

Based on the modal parameters of the developed jacket platform, the FRFs at different locations of the model have been calculated. Also, a large number of frequency points with the FRF values can be used as reference data to construct the cost function for model updating. However, Kwon et al. [37, 38] indicated that some of frequency ranges were considered redundant for model updating. In the present study, the certain rules have been applied to constrain the frequency range selection based on the existing rules: (i) The frequencies around the resonance were selected due to the high sensitivity to the parameter variations of structures [26]. (ii) As the damping-induced FRFs amplitudes were highly attenuated away from the resonant region [39], the frequencies sufficiently far from the resonance were selected. (iii) To obtain a monotonic decrease of the response residual vector during the optimization process, the frequencies outside the region between the theoretical and measured resonances were selected for model updating [25]. The aforementioned observations have enabled an effective selection of the frequency range to guarantee the convergence of the optimization algorithm. Fig. 3 has shown an example of the frequency range selection for the calculations of acceleration FRF between the load at Point 12 and the response at Point 1 of the jacket platform model under the consideration of the above rules.

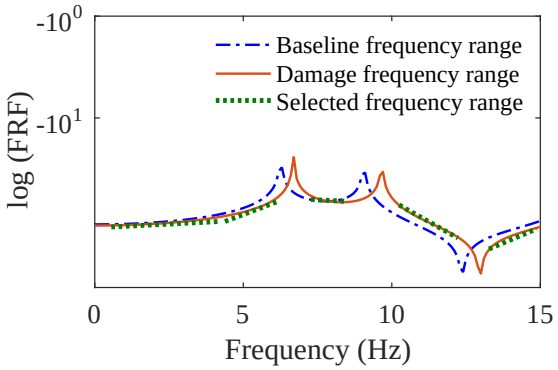

Fig. 3: Frequency range selection of the FRF.

4.2. Synergy of RBD-FAST and IPSO for model updating

Following the mathematical derivation in Section 3.3, sensitivity analysis of the variation coefficients using the RBD-FAST method has been conducted to determine the key parameters for the updating. As shown in Fig. 4, the remarkable difference of the first-order sensitivity between the stiffness and mass variation coefficients of the jacket platform model has been observed. It has been noted that the highest sensitivity index of stiffness variation coefficients is larger than that of mass variation coefficients by 39.04%. It has been also observed that the high sensitivity indices of stiffness variation coefficients are clustered in the vicinity of the elements labelled as 31 and 48, which represents the bars at the bottom of the jacket platform. Furthermore, results have demonstrated that the deteriorated stiffness near the fixture has caused the noticeable variations of the cost function in Eq. (11), where the structural natural frequencies and the SACs of FRFs have been formulated.

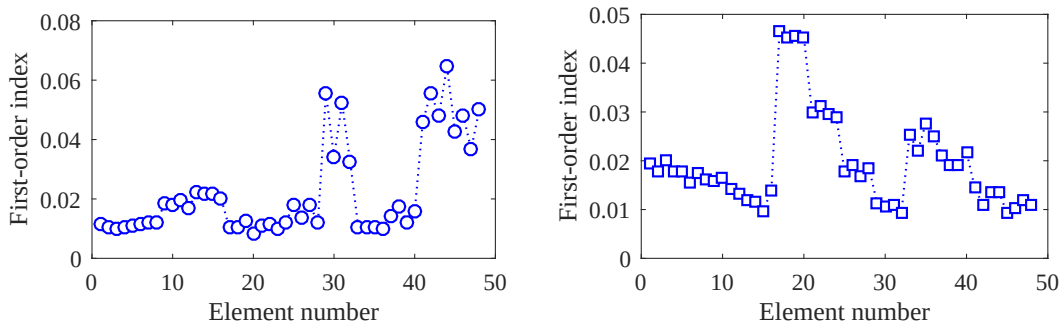

Fig. 4: First-order sensitivity of variation coefficients for the jacket platform: (a) Stiffness variation coefficients, (b) Mass variation coefficients.

In order to achieve a well-balanced between the time cost and convergence of the global optimization process, the variation coefficients of the elements have been ranked from lowest to highest according to the sensitivity index values calculated by RBD-FAST, and the last twenty ranked variation coefficients have been selected as the key parameters for the model updating. The remaining parameters have been ignored for the updating due to the assumption that no

damage has occurred. In the entire optimization process, the population size and number of iterations for the IPSO algorithm have been set as 500 and 100, respectively. The other parameters configuration of the IPSO method has been shown in Table. 1. The optimization results by the synergy of RBD-FAST and IPSO have been shown in Fig. 5. It can be observed that the proposed method has the capability to obtain the correct variation coefficients during the updating process, as results have been in good agreement with the theoretical values of the preset damage in the jacket platform. Therefore, the accuracy and effectiveness of the sensitivity-assisted IPSO for model updating have been validated.

Table 1: Parameters configuration of the IPSO method.

Inertia weight	Maximum value ($\widehat{\omega}_{\max}$)	Minimum value ($\widehat{\omega}_{\min}$)
	0.9	0.4
Learning factors	Initial values ($c_{1,ini}$ and $c_{2,ini}$)	Final values ($c_{1,fin}$ and $c_{2,fin}$)
	0.5 and 0.6	2.5

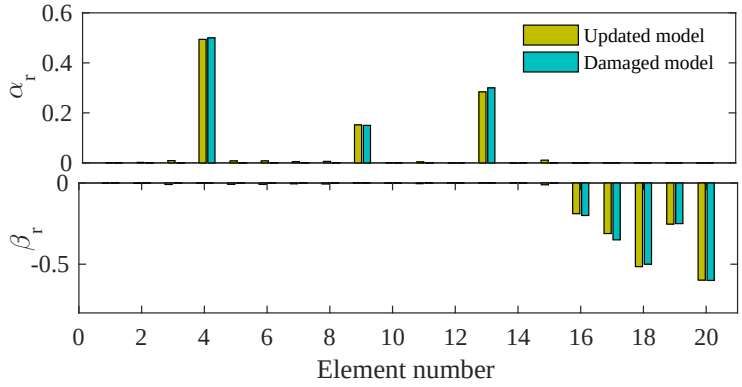

Fig. 5: The updated variation coefficients for the jacket platform.

5. Model updating of the 4 MW offshore wind turbine benchmark

In this section, the field data from the 4MW offshore wind turbine benchmark under various working conditions has been explored to extract the time-varying acceleration components (TVAC) for the construction of mode shapes. Furthermore, the feasibility of the proposed method for model updating of the 4MW offshore wind turbine benchmark has been validated. Finally, the remarkable advantages of the synergy of RBD-FAST and IPSO including the accuracy, stability, and computational efficiency have been comprehensively discussed and concluded.

5.1. *Field testing of the 4MW offshore wind turbine benchmark*

To verify the effectiveness of the proposed method in solving the practical engineering problems, the field test has been conducted on the 4MW offshore wind turbine benchmark called 37#OWT (N32°50′, E121°31′), which has been located approximately 44 km off the coast of Rudong, Jiangsu Province. Five 3-axis MEMS (Micro Electro Mechanical Systems) acceleration sensors used for signal measurement have been mounted on the inner wall of the tower in Fig. 6 at different heights of 13m (Level 1), 25m (Level 2), 58m (Level 3), 79m (Level 4) and 93m (Level 5), respectively. The vibration signals measured by acceleration sensors have been acquired using the CANSAS-SC8I data acquisition instrument (IMC, Germany) with a sampling interval of 0.005s.

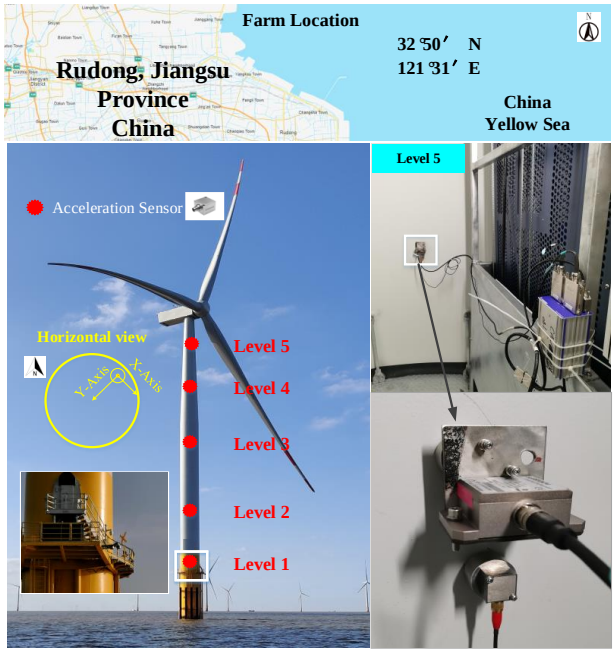

Fig. 6: The layout of acceleration sensors for the 37#OWT in the field testing.

In order to better differentiate the acceleration signals obtained, it is necessary to classify the service conditions, in which the 4MW offshore wind turbine benchmark has worked in the field test. Based on the supervisory control data acquisition (SCADA) system that has the ability to accurately describe operating conditions of the rotor, four types of scenarios have been clearly developed, including normal operating scenario (Scenario I), shutdown scenario (Scenario II), ship collision scenario (Scenario III) and typhoon scenario (Scenario IV) in Fig. 7.

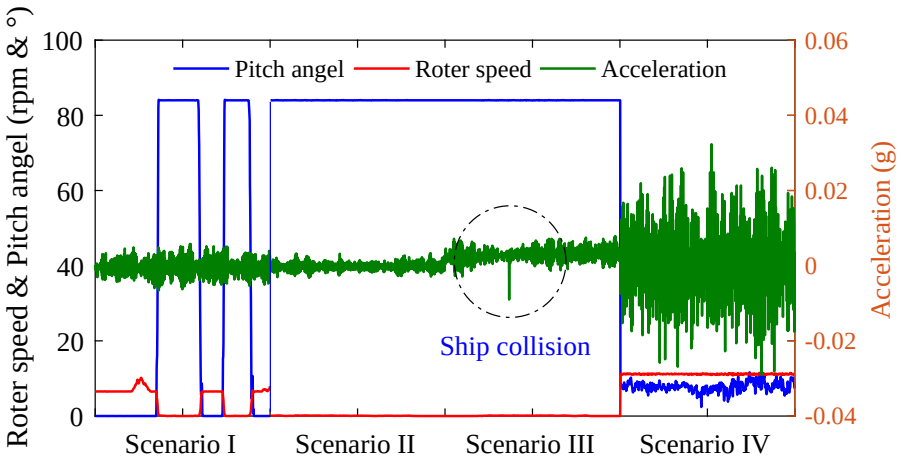

Fig. 7: The classification of service scenarios for 37#OWT.

Taking the point at Level 1 as an example, the measured horizontal acceleration signals in the normal operating and ship collision scenarios have been shown in Fig. 8.

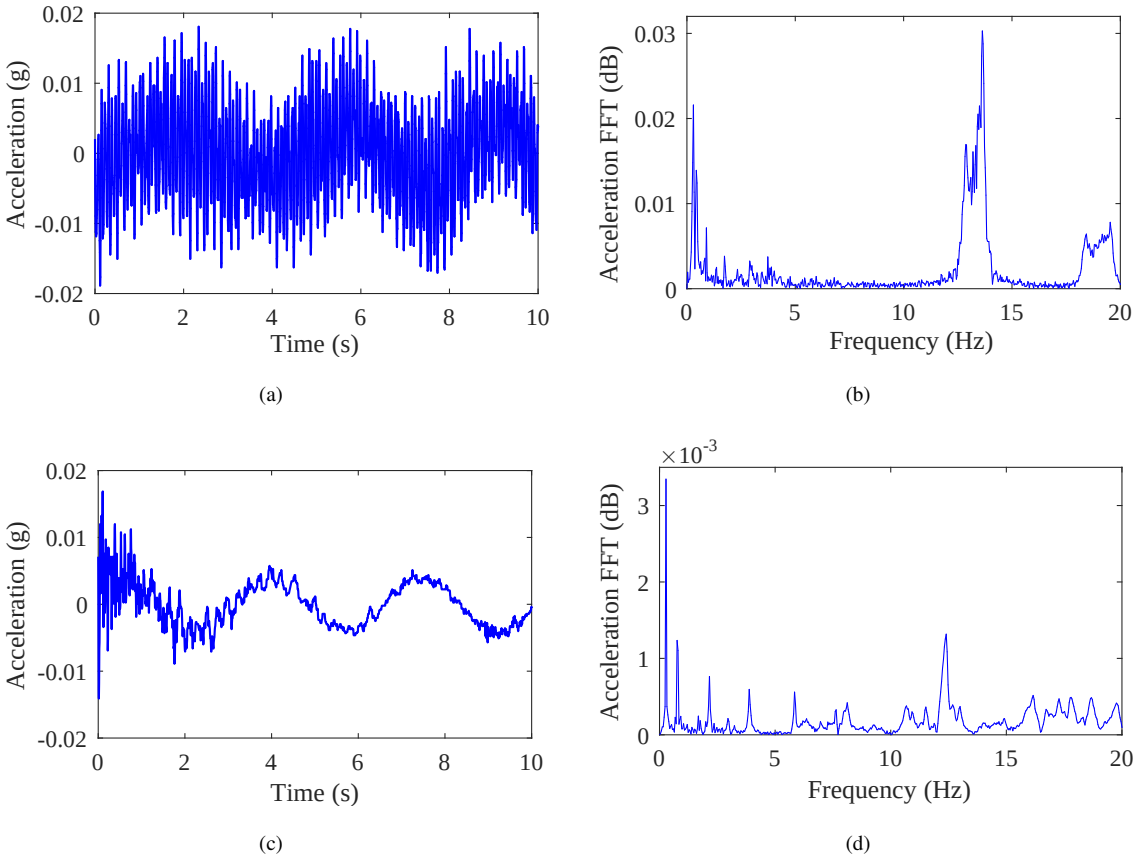

Fig. 8: Measured acceleration signals at Level 1: (a) Normal operating scenario in time domain , (b) Normal operating scenario in frequency domain, (c) Ship collision scenario in time domain, (d) Ship collision scenario in frequency domain.

The acceleration amplitude extracted in the normal operating scenario has been averagely higher as compared to that obtained in the ship collision scenario as shown in Fig. 8(a), indicating that the vibration response has been stronger under the combined action from wind, waves and aerodynamic loads in the normal operating scenario. When the collision has occurred, the acceleration response has reached the maximum amplitude of 0.0187g within the first 2s and then has decayed rapidly shown in Fig. 8(c). As the acceleration amplitude has reached its trough, it has noted that aerodynamic loads acting on blades has been weakened by the downward pitch. Usually, the energy of a signal in the frequency domain has been distributed with frequency, indicating the critical information of the system and structural loads. By the comparison of results in Fig. 8(b), more prominent peaks have been observed in Fig. 8(d) and more effective modal characteristics about the 37#OWT have been represented in the ship collision scenario. It has been also noted that the energy of the acceleration response is more prone to be affected by noise due to the low ratio of the signal to the interference plus noise in the normal operating scenario. As the shutdown has eliminated the mechanical disturbance of the blades to the tower, the vibration signals containing little noise have been obtained in the collision scenario in Fig. 8(d).

5.2. Model updating based on measured data

As discussed in Section 3.1, the TVAC that can be used to construct the acceleration FRFs have been the key step in developing the mathematical formulation of the cost function. It is vital to accurately extract the TVAC, which has been seen as the crucial indicators for evaluating the real state of structures. As shown in Fig. 9, the TVAC has represented the variation of structural vibration characteristics with time, and the first-two orders normalized TVAC of 37#OWT also has achieved a good agreement with the theoretical mode shapes. Furthermore, the discrepancy of different normalized TVAC has been illustrated in Fig. 10. As the ambient load excitation is small, only the first-order normalized TVAC of the structures in the shutdown scenario has been extracted. Under the collision and typhoon working conditions, the first-three orders normalized TVAC of 37#OWT has been provided due to the intense excitation forces.

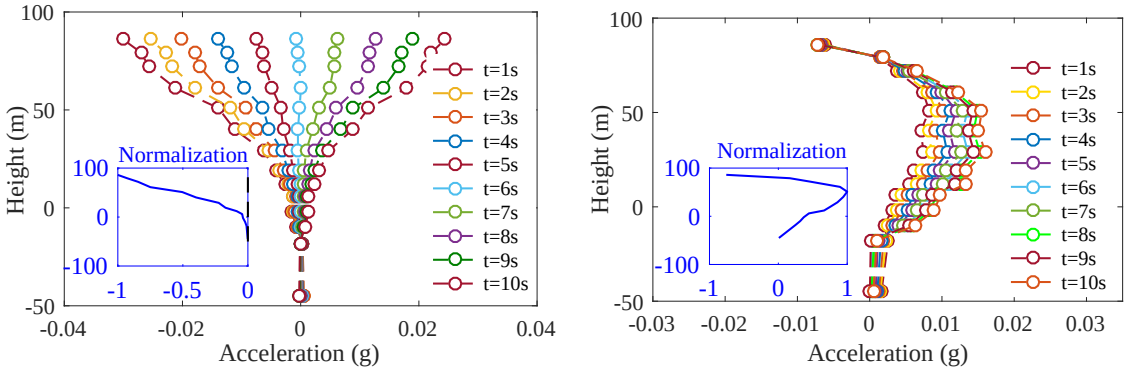

Fig. 9: The TVAC in the normal operating scenario: (a) 1-st TVAC, (b) 2-nd TVAC.

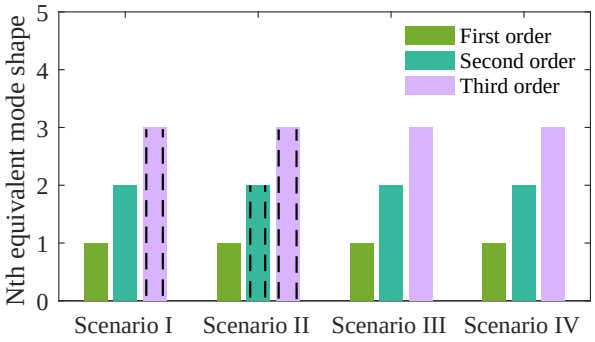

Fig. 10: The number of normalized TVAC.

The comparison results of the obtained first-order normalized TVAC considering various rotor speeds and working conditions have been shown in Fig. 11, demonstrating the time-varying performance of the 4MW offshore wind turbine benchmark. It has been worthy of noting that the discrepancy of results on the first-order normalized TVAC

has been increased in the different scenarios as compared with that obtained by different rotational speeds, indicating the stronger sensitivity of structural variations to service working conditions over the rotor speeds. In summary, the above results have demonstrated effectiveness and accuracy of the extracted the TVAC from acceleration signals for model updating.

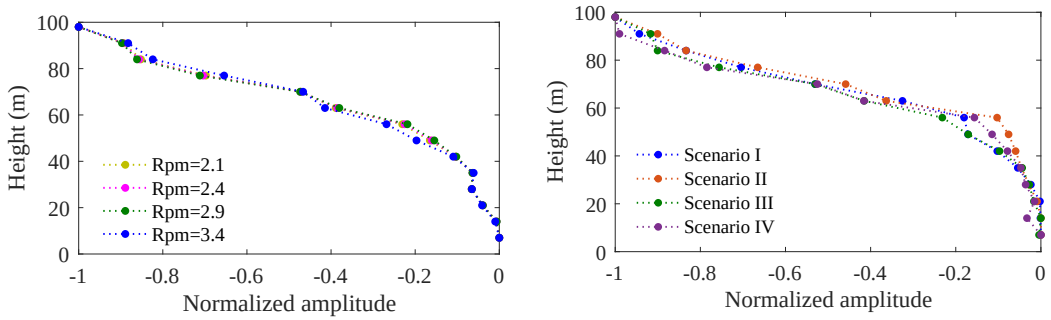

(a) (b)

Fig. 11: Comparison results of the first-order normalized TVAC: (a) Slightly varying rotational speeds, (b) Multiple scenarios.

To determine key parameters of the 4MW offshore wind turbine benchmark during the updating process, the RBD-FAST method has been used to analyze the sensitivity of stiffness and mass variation coefficients. It has been worth mentioning that in the reference model of 37#OWT, as 53 beam elements modelled by ABAQUS have been used, there have been 106 variation coefficients for sensitivity analysis to be determined. In Fig. 12, the first-order sensitivity of variation coefficients for different elements has been provided. The higher sensitivity index value of stiffness variation coefficients has been observed than that of the mass variation coefficients. Meanwhile, the fluctuation trend of the sensitivity index value for stiffness variation coefficients has shown the first-order index variation along with the change in element positions from top to bottom along the 37#OWT in Fig. 12(a). The closer to the bottom element, the first-order index increases greatly. More specifically, three sensitivity indices of stiffness variation coefficients for elements near the restrained end of 37#OWT have been calculated with the values of 0.39, 0.19 and 0.08 respectively. These indices are much higher than those of the other elements. It has been concluded that the amplitude of the sensitivity index for the mass variation coefficients has been smaller in Fig. 12(b) as compared with those of the stiffness variation coefficients, revealing that the mass is of less importance and concern in the model updating.

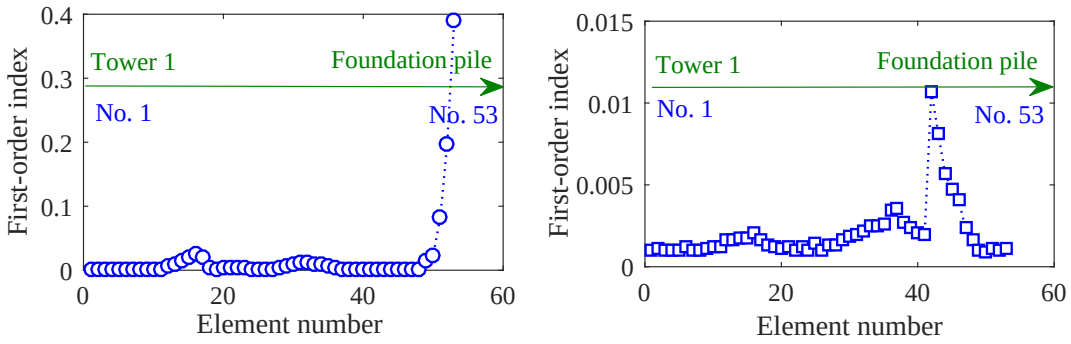

Fig. 12: First-order sensitivity of variation coefficients for 37#OWT: (a) Stiffness variation coefficients, (b) Mass variation coefficients.

Taking into account the balance between the efficiency and accuracy of the proposed method for the model updating, the variation coefficients $\mathbb{C}_{\text{ranking}}$ ranked in the top twenty five sensitivity index values in Eq. (23) have been selected as the critical parameters for the update of the 4MW offshore wind turbine benchmark. The convergence results calculated by the sensitivity-assisted IPSO method have been shown in Fig. 13, demonstrating that the cost function has been decreased rapidly at the 28th , 29th , 27th and 39th iteration in Scenarios I, II, III and IV, respectively. As compared with results in the other scenarios, the proposed method has reached the best cost function of 1.721 in the collision scenario, demonstrating the potential benefit when considering the collision condition applicable to model updating.

$$\mathbb{C}_{\text{ranking}} = \begin{bmatrix} \alpha_{18} & \beta_{45} & \alpha_{36} & \alpha_{20} & \beta_{44} \\ \alpha_{29} & \alpha_{12} & \alpha_{35} & \beta_{43} & \alpha_{30} \\ \alpha_{34} & \alpha_{33} & \alpha_{13} & \beta_{42} & \alpha_{31} \\ \alpha_{32} & \alpha_{49} & \alpha_{14} & \alpha_{17} & \alpha_{15} \\ \alpha_{50} & \alpha_{16} & \alpha_{51} & \alpha_{52} & \alpha_{53} \end{bmatrix} \tag{23}$$

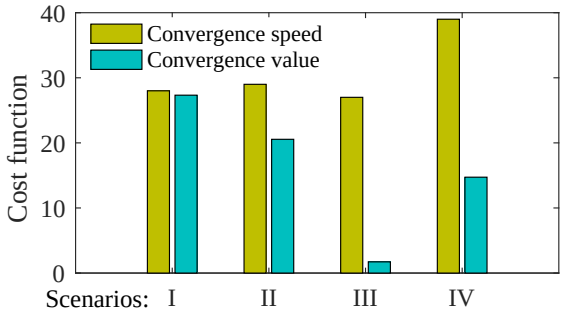

Fig. 13: Convergence performance in different scenarios.

As the 4MW offshore wind turbine benchmark has exhibited dynamic under the various working conditions, the

final updated results of stiffness and mass variation coefficients have shown variability for the four scenarios as shown in Fig. 14. The high values of stiffness variation coefficients have been mainly clustered in the 10th (α_{30}), 19th (α_{17}) and 22nd (α_{16}) elements in Scenario IV, indicating the change in the location of the updated parameters in the 4MW offshore wind turbine benchmark. Moreover, the number of stiffness variation coefficients has far exceeded that of mass variation coefficients, illustrating the greatest importance of updating the stiffness parameters in the model updating process.

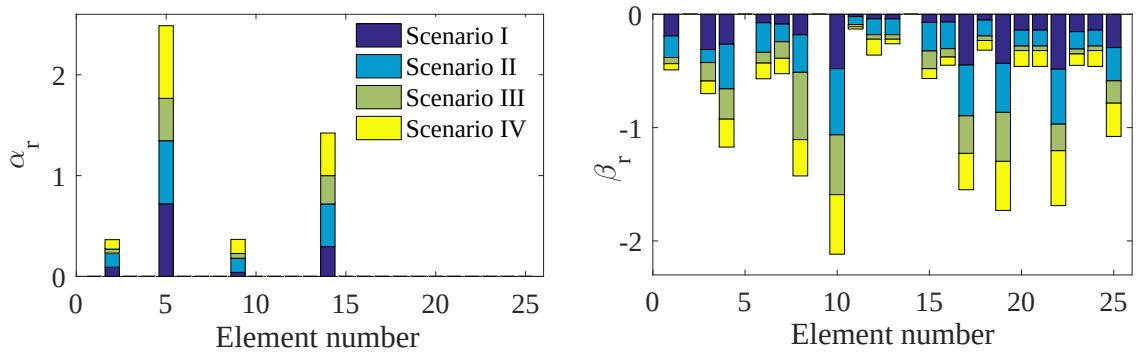

(a) (b)

Fig. 14: The updated variation coefficients in different scenarios: (a) Mass variation coefficients, (b) Stiffness variation coefficients.

To evaluate the correctness of the updated offshore wind turbine model, comparison results of natural frequencies among the benchmark model, the reference model and updated model in the four scenarios have been shown in Table 2. It has been noted that relative errors of the first-order natural frequency between the benchmark and updated model have been observed as 2.6127%, 0.2463%, 0.8970% and 1.1918% in Scenario I, II, III and IV, respectively. This has demonstrated the validity and accuracy of the proposed method in solving real marine engineering structures. As only the first-order TVAC has been extracted in the shutdown scenario, the relative errors of the second and third-order natural frequencies between the updated model and 4MW offshore wind turbine benchmark have not been effectively estimated. It has been worth noting that the relative errors of the first three natural frequencies between the updated model and 37#OWT in the collision scenario have reached the minimum values of 0.8970%, 0.1071% and 0.2096%, respectively. It could be reasonably interpreted by the result in Fig. 8(d), that is to say, the acceleration response used to extract real modal parameters in the collision scenario has contained little noise components.

Table 2: Comparison results of natural frequencies in different scenarios.

Scenarios	Natural frequency (Hz)	Benchmark model	Reference model	Relative error (%)	Updated model	Relative error (%)
Scenario I	1st	0.2794	0.2948	5.5118%	0.2721	2.6127%
	2nd	1.7292	1.9899	15.0763%	1.7272	0.1157%
	3rd	N/A	5.0597	N/A	4.5823	N/A
Scenario II	1st	0.2842	0.2948	3.7298%	0.2849	0.2463%
	2nd	N/A	1.9899	N/A	1.9529	N/A
	3rd	N/A	5.0597	N/A	4.7600	N/A
Scenario III	1st	0.2787	0.2948	5.7768%	0.2812	0.8970%
	2nd	1.8667	1.9899	6.5999%	1.8687	0.1071%
	3rd	4.6763	5.0597	8.1988%	4.6665	0.2096%
Scenario IV	1st	0.2769	0.2948	6.4644%	0.2802	1.1918%
	2nd	1.7370	1.9899	14.5596%	1.8040	3.8572%
	3rd	4.5222	5.0597	11.8858%	4.5619	0.8779%

Furthermore, the FRF ($\hat{H}_a^{31}$) between the 37#OWT and the updated model has been shown in Fig. 15. It has been noted that a number of resonances are closely spaced in the frequency regions where with the values of the FRFs, exhibiting complex modal characteristics of the 4MW offshore wind turbine benchmark. Meanwhile, the excellent agreement of FRF results between the updated model and the 37#OWT in the four scenarios has been observed. This has demonstrated the accuracy of the proposed method applied to the model updating. More specifically, the FRFs values between the benchmark and updated model have shown a slight difference when the frequency is within 1 Hz in the collision and typhoon scenarios. As this discrepancy has become pronounced in the operation scenario, where the relative error of the first-order natural frequency between the benchmark and updated model has been compared in Table 2. Finally, the RMSE (Root Mean Square Errors) of the FRFs values has been calculated to indicate more accurate results over the frequency interval achieved in the collision scenario as compare with that obtained in others scenarios.

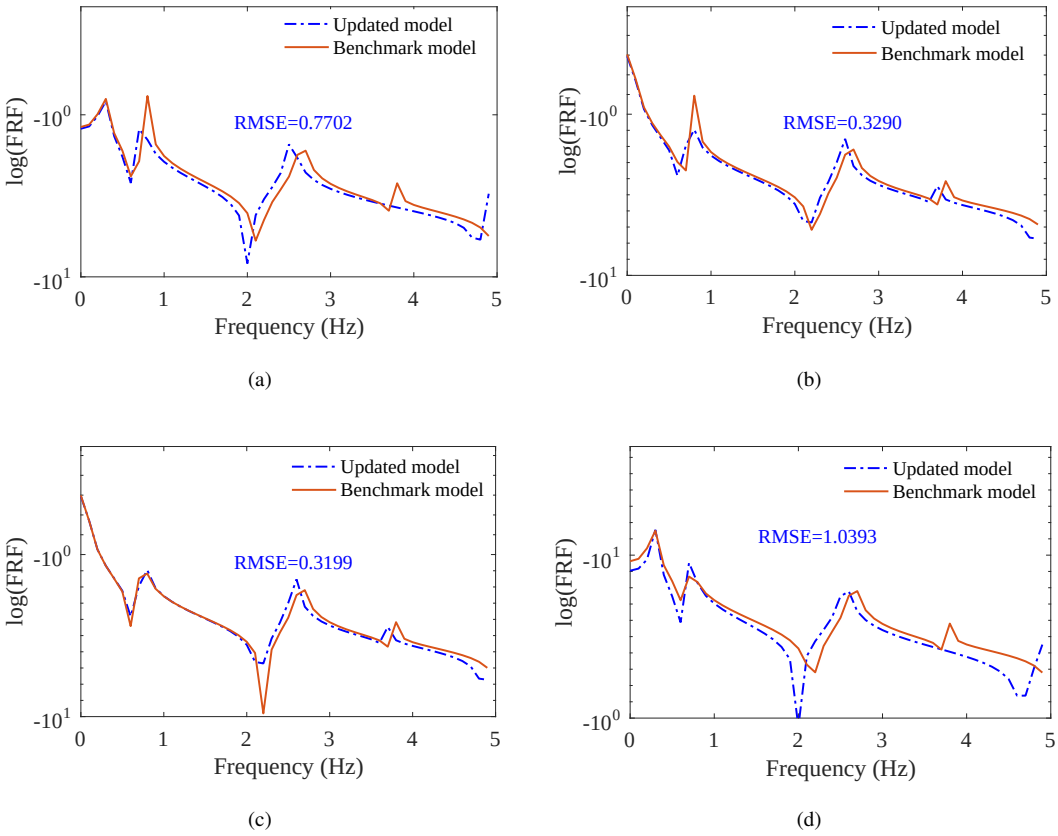

Fig. 15: Comparison results of FRFs in different scenarios: (a) Normal operating scenario , (b) Shutdown scenario, (c) Ship collision scenario, (d) Typhoon scenario.

5.3. Robustness analysis of sensitivity-based IPSO

To evaluate the robustness of the proposed method for model updating of the 4MW offshore wind turbine benchmark, the reference model has been updated under the consideration of conditions including the four scenarios and rotor speeds varying in the range of 2.1 to 3.4 rpm. In the stability analysis, the results obtained by the sensitivity-based IPSO have been computed 10 times in each service condition. The top 10 variation coefficients have been selected in the statistical analysis.

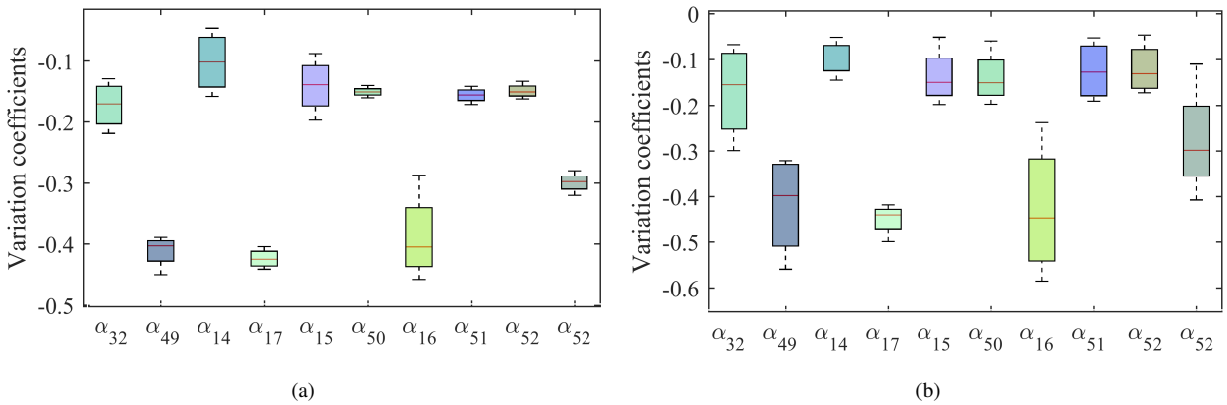

Fig. 16: Robustness of updated variation coefficients: (a) Slightly varying rotational speeds , (b) Multiple scenarios.

As shown in Fig. 16, the updated parameters have shown a slight variation in four service conditions, demonstrating the robustness of the synergy of RBD-FAST and intelligent IPSO in solving 4MW offshore wind turbine benchmark. As compared with the magnitudes of variation coefficients obtained in the minor range of rotor speeds, the larger bounds of variation coefficients have been achieved in four scenarios, indicating the more remarkable change of dynamic performances of offshore wind turbines across the multiple service conditions. In summary, the obtained results have demonstrated the robustness of the proposed method applied to the model updating of marine engineering structures.

5.4. Comparison results of model updating by different methods

In this section, the proposed method has been investigated for comparison of the typical methods including PSO and IPSO approach to highlight the superior performance in the process of model updating. As shown in Table 3, the sensitivity-based IPSO has efficiently reached the optimal solution at the 27th iteration as compared with the 42nd and 33rd iterations by PSO and IPSO, respectively. It should be also noted that the cost function of the proposed method has reached the minimum discrepancy of 1.721 between the updated model and the benchmark model. From the viewpoint of the computational cost, the tremendous amount of time has been consumed by PSO and IPSO (9535s and 9668s on a computer with the specifications of Intel I7 processor 3.60GHz and 32GB RAM, respectively) to find the best solution, while the shorter time of 7545s has been achieved by the proposed method. Due to the few numbers of variation coefficients in model updating, the synergy of RBD-FAST and IPSO has greatly reduced the time cost throughout the optimization process.

Table 3: Evaluation indicators of comparison results by different methods.

Evaluation indicators	PSO [40]	IPSO	RBD-FAST assisted IPSO
The number of iteration	100	100	100
Speed of convergence	42	33	27
Total times (s)	9535	9668	7545
Value of convergence	3.328	2.913	1.721

Natural frequencies obtained by three methods in Table 4 have also been compared between the 4MW offshore wind turbine benchmark and the updated model. The relative error of the first-order natural frequency calculated by PSO between the benchmark model and the updated model has reduced from 3.5163% to 3.2652% by IPSO, owing to the improved in weights and learning factors. It has been also noted that the smallest relative errors (0.8970%, 0.1071% and 0.2096%) of the first-three natural frequencies have been achieved in the proposed method as compared with the result by PSO and IPSO. A reason for this finding can be explained by the fact that the critical parameters selected by RBD-FAST for model updating have led to the fast convergence and high accuracy in the proposed method. Summarily, comparison results have demonstrated the effectiveness and correctness of the proposed method for model updating of offshore engineering structures subject to complex loads in various marine environments.

Table 4: Comparison results of natural frequencies by different methods.

Methods	Natural frequency (Hz)	Benchmark model	Updated model	Relative error (%)
PSO	1st	0.2787	0.2689	3.5163
	2nd	1.8667	1.8696	0.1554
	3rd	4.6763	4.4794	4.2106
IPSO	1st	0.2787	0.2696	3.2652
	2nd	1.8667	1.8692	0.1339
	3rd	4.6763	4.5676	2.3244
Synergy of RBD-FAST and IPSO	1st	0.2787	0.2812	0.8970
	2nd	1.8667	1.8687	0.1071
	3rd	4.6763	4.6665	0.2096

6. Summary and conclusions

In this study, the synergy of random balance designs-assisted Fourier amplitude sensitivity test and IPSO has been proposed to leverage the adaptive weights and dynamic learning factors for model updating of the 4MW offshore wind turbine benchmark subject to the various service conditions. The prominent advantages of the proposed approach have been demonstrated by the successfully capturing sensitive parameters from a large number of stiffness and mass variation coefficients of the structure to increase the computational efficiency. Also, the issue of incomplete

modal parameters has been addressed by the combination of the time-varying acceleration components (TVAC) and theoretical mode shapes. Throughout the numerical example, the correctness of the sensitivity-based IPSO has been validated. To further assess its effectiveness in solving practical marine engineering structures, the proposed approach has demonstrated the good agreement of results by the updated model and 4MW offshore wind turbine benchmark in terms of the natural frequencies and FRFs values under the consideration of complex service scenarios. As the acceleration signal has contained less noise in the extraction of the high orders TVAC, the minimum relative error (0.8970%) of the first natural frequency and the RMSE (0.3199) of FRF values between the benchmark and updated models in the ship collision scenario have been achieved by the proposed approach. As compared with the typical PSO and IPSO methods, the proposed method has been significantly improved in terms of fast convergence and accuracy. Moreover, results under the consideration of rotor speeds and various service scenarios have demonstrated the robustness of the proposed method applied to the model updating of 4MW offshore wind turbine benchmark. Based on these observations, the synergistic approach of RBD-FAST and IPSO has the power to accurately identify updating parameters of complex systems with the improved computational efficiency. Summarily, the updated results related to the 4MW offshore wind turbine benchmark under the various service conditions have demonstrated the feasibility and robustness of the proposed method, which has laid the foundation for the digital twinning realization of marine engineering structures.

7. Acknowledgements

The authors acknowledge the financial support of the National Outstanding Youth Science Fund Project of National Natural Science Foundation of China (52125106), the National Natural Science Foundation project (U22A20243) and the National Natural Science Foundation project (52001291).

References

[1] S. Cong, S.-L. J. Hu, H.-J. Li, Using incomplete complex modes for model updating of monopiled offshore wind turbines, Renewable Energy 181 (2022) 522–534. doi:10.1016/j.renene.2021.09.022.

[2] A. Mojtahedi, M. L. Yaghin, Y. Hassanzadeh, M. Ettefagh, M. Aminfar, A. Aghdam, Developing a robust SHM method for offshore jacket platform using model updating and fuzzy logic system, Applied Ocean Research 33 (4) (2011) 398–411. doi:10.1016/j.apor.2011.05.001.

[3] A. A. Elshafey, M. R. Haddara, H. Marzouk, Damage detection in offshore structures using neural networks, Marine Structures 23 (1) (2010) 131–145. doi:10.1016/j.marstruc.2010.01.005.

[4] E. Gavassoni, P. B. Gonçalves, D. de Mesquita Roehl, Nonlinear vibration modes of an offshore articulated tower, Ocean Engineering 109 (2015) 226–242. doi:10.1016/j.oceaneng.2015.08.028.

[5] A. Fathi, A. Esfandiari, M. Fadavie, A. Mojtahedi, Damage detection in an offshore platform using incomplete noisy FRF data by a novel bayesian model updating method, Ocean Engineering 217 (2020) 108023. doi:10.1016/j.oceaneng.2020.108023.

[6] Q. Cao, H. Li, H. Li, F. Liu, Time-dependent reliability analysis of fixed offshore structures under stochastic loadings, Applied Ocean Research 117 (2021) 102901. doi:10.1016/j.apor.2021.102901.

[7] S. Chang, F. Liu, X. Ji, A tracking method of equivalent constraint boundary for offshore monopile wind turbines from measured accelerations, Ocean Engineering 256 (2022) 111391. doi:10.1016/j.oceaneng.2022.111391.

[8] A. Berman, E. J. Nagy, Improvement of a large analytical model using test data, AIAA Journal 21 (8) (1983) 1168–1173. doi:10.2514/3.60140.

[9] A. Berman, Mass matrix correction using an incomplete set of measured modes, AIAA Journal 17 (10) (1979) 1147–1148. doi:10.2514/3.61290.

[10] M. Baruch, Optimal correction of mass and stiffness matrices using measured modes, AIAA Journal 20 (11) (1982) 1623–1626. doi:10.2514/3.7995.

[11] M. Baruch, Optimization procedure to correct stiffness and flexibility matrices using vibration tests, AIAA Journal 16 (11) (1978) 1208–1210. doi:10.2514/3.61032.

[12] H. Natke, Updating computational models in the frequency domain based on measured data: a survey, Probabilistic Engineering Mechanics 3 (1) (1988) 28–35. doi:10.1016/0266-8920(88)90005-7.

[13] X.-Q. Zhou, Y. Xia, S. Weng, L1 regularization approach to structural damagedetection using frequency data, Structural Health Monitoring 14 (6) (2015) 571–582. doi:10.1177/1475921715604386.

[14] S. Wang, Damage detection in offshore platform structures from limited modal data, Applied Ocean Research 41 (2013) 48–56. doi:10.1016/j.apor.2013.02.004.

[15] Z.-Q. Qu, Adaptive mode superposition and acceleration technique with application to frequency response function and its sensitivity, Mechanical Systems and Signal Processing 21 (1) (2007) 40–57. doi:10.1016/j.ymssp.2006.02.002.

[16] A. Esfandiari, F. Bakhtiari-Nejad, A. Rahai, Theoretical and experimental structural damage diagnosis method using natural frequencies through an improved sensitivity equation, International Journal of Mechanical Sciences 70 (2013) 79–89. doi:10.1016/j.ijmecsci.2013.02.006.

[17] Y. Xu, W. Zhu, S. Smith, Non-model-based damage identification of plates using principal, mean and gaussian curvature mode shapes, Journal of Sound and Vibration 400 (2017) 626–659. doi:10.1016/j.jsv.2017.03.030.

[18] Y. Zhang, L. Wang, Z. Xiang, Damage detection by mode shape squares extracted from a passing vehicle, Journal of Sound and Vibration 331 (2) (2012) 291–307. doi:10.1016/j.jsv.2011.09.004.

[19] S. Quqa, L. Landi, P. P. Diotallevi, Automatic identification of dense damage-sensitive features in civil infrastructure using sparse sensor networks, Automation in Construction 128 (2021) 103740. doi:10.1016/j.autcon.2021.103740.

[20] J. Naranjo-Pérez, M. Infantes, J. F. Jiménez-Alonso, A. Sáez, A collaborative machine learning-optimization algorithm to improve the finite element model updating of civil engineering structures, Engineering Structures 225 (2020) 111327. doi:10.1016/j.engstruct.2020.111327.

[21] K. Tiwary, S. K. Patro, A. H. Gandomi, K. S. Sahoo, Model updating using causal information: a case study in coupled slab, Structural and Multidisciplinary Optimization 65 (2). doi:10.1007/s00158-021-03166-w.

[22] F. Liu, S. Gao, S. Chang, Displacement estimation from measured acceleration for fixed offshore structures, Applied Ocean Research 113 (2021) 102741. doi:10.1016/j.apor.2021.102741.

[23] A. Esfandiari, Structural parameter estimation and damage detection using experimental transfer function data, Inverse Problems in Science and Engineering 28 (1) (2019) 2–20. doi:10.1080/17415977.2019.1568426.

[24] A. K. Panda, S. V. Modak, An FRF-based perturbation approach for stochastic updating of mass, stiffness and damping matrices, Mechanical Systems and Signal Processing 166 (2022) 108416. doi:10.1016/j.ymssp.2021.108416.

[25] S. Hassani, F. Shadan, Using incomplete FRF measurements for damage detection of structures with closely-spaced eigenvalues, Measurement 188 (2022) 110388. doi:10.1016/j.measurement.2021.110388.

[26] F. Shadan, F. Khoshnoudian, A. Esfandiari, A frequency response-based structural damage identification using model updating method, Structural Control and Health Monitoring 23 (2) (2015) 286–302. doi:10.1002/stc.1768.

[27] J. Wang, C. Wang, J. Zhao, Frequency response function-based model updating using kriging model, Mechanical Systems and Signal Processing 87 (2017) 218–228. doi:10.1016/j.ymssp.2016.10.023.

[28] L. Prendergast, W. Wu, K. Gavin, Experimental application of FRF-based model updating approach to estimate soil mass and stiffness mobilised under pile impact tests, Soil Dynamics and Earthquake Engineering 123 (2019) 1–15. doi:10.1016/j.soildyn.2019.04.027.

[29] H. Ouyang, J. Liu, Z. Li, X. Han, A novel dynamic model updating method for composite laminate structures considering non-probabilistic uncertainties and correlations, Composite Structures 287 (2022) 115359. doi:10.1016/j.compstruct.2022.115359.

[30] W. Zhong, Z. Chen, Model updating method for hybrid simulation based on global sensitivity analysis, Earthquake Engineering and Structural Dynamics 50 (14) (2021) 3792–3813. doi:10.1002/eqe.3533.

[31] T. A. Mara, Extension of the RBD-FAST method to the computation of global sensitivity indices, Reliability Engineering and System Safety 94 (8) (2009) 1274–1281. doi:10.1016/j.ress.2009.01.012.

[32] J. Goffart, M. Woloszyn, EASI RBD-FAST: An efficient method of global sensitivity analysis for present and future challenges in building performance simulation, Journal of Building Engineering 43 (2021) 103129. doi:10.1016/j.jobe.2021.103129.

[33] A. Esfandiari, M. Sanayei, More insight on function-weighted frequency response function sensitivity method for analytical model updating, Journal of Sound and Vibration 509 (2021) 116143. doi:10.1016/j.jsv.2021.116143.

[34] T. Zhu, G. Zhang, C. Zang, Frequency-domain nonlinear model updating based on analytical sensitivity and the multi-harmonic balance method, Mechanical Systems and Signal Processing 163 (2022) 108169. doi:10.1016/j.ymssp.2021.108169.

[35] X. Li, F. Liu, A nonmode-shape-based model updating method for offshore structures using extracted components from measured accelerations, Applied Ocean Research 121 (2022) 103087. doi:10.1016/j.apor.2022.103087.

[36] S. Ghosh, S. Das, D. Kundu, K. Suresh, B. K. Panigrahi, Z. Cui, An inertia-adaptive particle swarm system with particle mobility factor for improved global optimization, Neural Computing and Applications 21 (2) (2010) 237–250. doi:10.1007/s00521-010-0356-x.

[37] K.-S. Kwon, R.-M. Lin, Frequency selection method for FRF-based model updating, Journal of Sound and Vibration 278 (1-2) (2004) 285–306. doi:10.1016/j.jsv.2003.10.003.

[38] M. I. Friswell, J. E. Mottershead, Finite Element Model Updating in Structural Dynamics, Springer Netherlands, 1995. doi:10.1007/978-94-015-8508-8.

[39] A. Esfandiari, F. Bakhtiari-Nejad, A. Rahai, M. Sanayei, Structural model updating using frequency response function and quasi-linear sensitivity equation, Journal of Sound and Vibration 326 (3-5) (2009) 557–573. doi:10.1016/j.jsv.2009.07.001.

[40] Y. Kang, Z. Qiu, H. Zhang, Z. Shi, F. Gu, Model updating for rotor-discs system and its application in dynamic coefficients identification of journal bearings, Measurement 173 (2021) 108645. doi:10.1016/j.measurement.2020.108645.